

## HD 91805 AND THE NATURE OF THE BIDELMAN-MACCONNELL WEAK-G-BAND STARS

P. L. COTTRELL AND JOHN NORRIS

Mount Stromlo and Siding Spring Observatory, Research School of Physical Sciences,  
The Australian National University

Received 1977 September 6; accepted 1977 November 7

### ABSTRACT

High-dispersion spectra of the weak-G-band star HD 91805 and DDO intermediate-band photometry of a number of the weak-G-band stars of Bidelman and MacConnell have been analyzed, and lead to the following results: (i) For HD 91805,  $[Fe/H] \sim 0.0$ ,  $[C/H] \sim -1.4$ ,  $[N/H] \sim +0.6$ , and  $[O/H] \sim +0.1$ . The simplest explanation of these abundance ratios is that material processed in the CN cycle (but not the NO cycle) has been introduced into the surface layers. (ii) The majority of the Bidelman-MacConnell objects are in the same phase of evolution as the Hyades clump stars. They are probably core helium-burning objects, subsequent to the helium flash. (iii) Consideration of several mechanisms (the helium core flash, mass loss, thermal instability of hydrogen-burning shells, the Paczyński mechanism of N/C enhancement by meridional circulation) suggests that the Paczyński mechanism coupled with moderate mass loss alone invokes no radical postulates and violates none of the observational constraints.

*Subject headings:* nucleosynthesis — stars: abundances — stars: individual — stars: late-type — stars: weak-line

### I. INTRODUCTION

Stars which possess anomalously weak CH bands (the weak-G-band stars) appear to exist in all populations. The peculiarity was first recognized by Cannon (1912) and Bidelman (1951) in HR 885, the Population I prototype. Eggen (1971) places HD 191046, another member of the class (Greenstein and Keenan 1958), in the Arcturus group. The existence of weak-G-band stars in the halo was first recognized by Zinn (1973), who discovered them in M92; his result appears to extend to all metal-poor globular clusters ( $[Fe/H] \leq -1.0$ ) (see Mallia 1975; Norris and Bessell 1977; Norris and Zinn 1977; Zinn 1977).

While no field halo stars are yet available for detailed (i.e., high-dispersion) analysis, more progress can be made in the younger populations. It is hoped that this will throw light on the phenomenon in Population II. Greenstein and Keenan (1958) first demonstrated that HR 885 is deficient in CH and CN by factors of  $\sim 30$  and  $\sim 100$ , respectively. Following the survey work of Bidelman and MacConnell (1973), some 40 weak-G-band stars are now recognized among field stars brighter than 10th mag. One of these, HR 6766, has recently been analyzed by Dean, Lee, and O'Brien (1977) and by Sneden and Peterson (1977). The latter authors find  $[Fe/H] \sim -0.25$ ,  $[C/Fe] \sim -1.3$ ,  $[N/Fe] \sim +0.8$ , and  $[O/Fe] \sim -0.1$ .

There is a growing consensus that the weak-G-band phenomenon in all populations results from the mixing of CNO processed material to the surface of these stars (Butler, Carbon, and Kraft 1975; Norris and Zinn 1977; Dean *et al.*; Sneden and Peterson 1977; Carbon *et al.* 1977). The site and details of the mixing process, however, are not yet clear. In an effort to

provide more information on this problem, we have obtained spectroscopic and photometric observations of the weak-G-band star HD 91805 together with intermediate-band photometry of a number of the Bidelman-MacConnell objects (§ II). In particular, we have performed curve-of-growth and spectrum synthesis analyses of the weak-G-band star HD 91805 to obtain an insight into the products of mixing (§ III); our results are very similar to those reported by Sneden and Peterson (1977) for HR 6766. In § IV we present evidence, based on DDO intermediate-band photometry, that the majority of the Bidelman-MacConnell weak-G-band stars are burning helium in their cores subsequent to the helium core flash. In the final section we consider possible causes of the weak-G-band anomaly, subject to the constraints deduced in the earlier sections. Of the mechanisms considered, carbon depletion due to meridional circulation (see Paczyński 1973) requires the least radical departure from now well understood astrophysical processes.

### II. OBSERVATIONS

#### a) Spectra

The weak-G-band star HD 91805 together with two Hyades giants HD 28307 (cluster) and HD 100407 (group) were observed with a variety of gratings and cameras available on the coude spectrograph of the 1.9 m telescope at Mount Stromlo.

High-dispersion spectra to be used in a curve-of-growth analysis were obtained by utilizing an échelle grating in combination with the 81 cm camera and a two-stage Carnegie image tube. The spectral range covered was from  $\lambda\lambda 5200$  to  $5500$  with a reciprocal

dispersion of  $\sim 1.5 \text{ \AA mm}^{-1}$ , and a wavelength range of  $\sim 50 \text{ \AA}$  per order. Good wavelength coverage was obtained for HD 91805 and HD 100407, but the data for HD 28307 were less extensive, and our method of analysis for this star will be discussed in § IIIa. We also used the échelle grating to obtain spectra in the region of the [O I] line at  $6300.3 \text{ \AA}$ ; the reciprocal dispersion was  $\sim 2.5 \text{ \AA mm}^{-1}$ .

The échelle grating was not particularly useful in obtaining spectra of the blue molecular features. Not only is its response function curved along a given order, but there are few (if any) continuum points in each order, making any effort at continuum placement quite imprecise. Therefore the G-band and the CN molecular feature running blueward of  $\lambda 4216$  were obtained directly (without image tube) by using the B grating in the second order and the 81 cm camera to give a reciprocal dispersion of  $10 \text{ \AA mm}^{-1}$ . Direct plates were obtained only for HD 91805 and HD 28307. However, for HD 100407 an échelle spectrum, with reciprocal dispersion of  $\sim 1 \text{ \AA mm}^{-1}$ , was obtained in the G-band region. This spectrum had a higher resolution,  $\sim 0.4 \text{ \AA}$ , than that found for the direct plate spectra. For the latter, the resolution was  $\sim 0.6 \text{ \AA}$ .

The CN feature near  $\lambda 3883$  was acquired with the C grating in the third order in combination with the 81 cm camera, and the image tube. The reciprocal dispersion of this combination was  $\sim 7 \text{ \AA mm}^{-1}$ ; 2 mm of BG3 was used to remove overlapping orders.

Finally, we obtained spectra of the NH features near  $\lambda 3360$  by using the C grating in the fourth order, together with a Carnegie image tube attached to the 40 cm camera. The reciprocal dispersion was  $\sim 10 \text{ \AA mm}^{-1}$ . Overlapping orders were removed by using 2 mm of UG5, together with 5 mm of a liquid  $\text{CuSO}_4$  solution.

For these last two regions, we were able to obtain data for HD 91805 and only one of the Hyades giants, HD 100407.

All data were recorded on Ila-O emulsion by using various methods of sensitization. The direct plates were obtained on baked plates, the NH and CN features on nitrogen-soaked plates, and the échelle plates on hydrogen-sensitized emulsions. Intensity calibrations were taken on separate plates, except for the direct plate, which carried its own calibration, and all were used to program the Göttingen microphotometer to give intensity tracings of the above spectra. Line strength measurements from these tracings, which form the basis of our curve-of-growth analysis, are given in the Appendix.

#### b) Photometry

DDO intermediate-band photometry has been obtained for 23 of the weak-G-band stars of Bidelman and MacConnell (1973). The observations were made with the 0.6 m telescope on Siding Spring Mountain in 1975 February and 1977 January. A 1P21 pulse-continuing photometer was employed, together with the equatorial standards of McClure (1976). The results are given in Table 1, where the columns are

self-explanatory. In the final row of the table we list the mean standard errors of our colors, derived from those stars having multiple observations.

In view of the fact that several of the DDO band-passes include features of the CN and CH molecule, the data in Table 1 are difficult to interpret. We believe, however, that an important result can be distilled from the results in the  $[C(42-45), C(45-48)]$ -plane. We refer to leave this discussion, however, until we have completed our abundance analysis of HD 91805, which we regard as a typical weak-G-band star.

### III. ANALYSIS OF HD 91805 WITH RESPECT TO TWO HYADES GIANTS

Our analysis is divided into two sections: (a) a differential curve-of-growth analysis, using Pagel's (1964) formulation as expressed by Griffin (1969) to determine the iron abundance and electron pressure of HD 91805; and (b) a detailed analysis of the following features: (1) the forbidden [O I] line at  $\lambda 6300.3$ ; (2) the G-band between  $\lambda \lambda 4290$  and  $4330$ ; (3) the wavelength interval  $\lambda \lambda 3870$  to  $3885$  which is dominated by two band heads of the blue CN system ( $\Delta v = 0$ ); (4) the section of spectrum from  $\lambda \lambda 4192$  to  $4217$  which contains two band heads of the  $\Delta v = -1$  blue CN system; and (5) the region  $\lambda \lambda 3356$  to  $3377$  which encompasses two band heads of the NH triplet system ( $A^3\Pi-X^3\Sigma$ ). This approach yields C, N, and O abundances in the atmosphere of the weak-G-band star HD 91805.

#### a) Curve-of-Growth Analysis

HD 91805 has been compared with two stars, HD 28307 and HD 100407. Both are members of the Hyades cluster or moving group, according to Eggen (1972) and Boyle and McClure (1975). Recently, Eggen (1977) has shown that HD 100407 may not be a member of the group. This, however, does not affect our analysis, since we determine all our parameters relative to HD 28307, a confirmed cluster member. Photometric data for the three stars (Eggen 1972) are given in Table 2, together with estimates of their atmospheric parameters, a discussion of which follows.

In our curve-of-growth treatment we make the basic assumption, following Griffin (1969), that  $\Delta\theta_{\text{exc}} \equiv \Delta\theta_{\text{ion}} \equiv \Delta\theta_{\text{eff}}$ ; the effective temperatures have been derived from the broad-band color  $(R-I)_K$ , using the transformations of Eggen (1972) and Johnson (1966) and are given in column (5) of Table 2.

Pagel's (1964) formula for the differential horizontal shift,  $[X_0]$ , of neutral lines of a particular element,  $j$ , relates this quantity to the differential abundance,  $[N_j/H]$ , of that species relative to hydrogen, by  $[X_0] = [\theta] + \Delta\theta(I_j - 0.74) + [N_j/H]$ , where  $I_j$  is the ionization potential of the element,  $j$ ; [...] refers to the logarithmic difference in each parameter.

The Arcturus curve of growth (van de Held's curve from Griffin and Griffin 1967) was fitted to all our curves, and is represented by the solid line in Figures 1 and 3.

TABLE 1  
DDO PHOTOMETRY OF 23 WEAK-G-BAND STARS

HD	C(45-48)	C(42-45)	C(41-42)	C(38-42)	n
18636	1.130	0.676	0.135	-0.385	1
21018	1.109	0.640	0.133	-0.516	1
BD+5 <sup>o</sup> 593	1.286	0.774	0.141	-0.281	3
26575	1.205	0.833	0.250	-0.209	3
28932	1.169	0.723	0.136	-0.406	3
BD-19 <sup>o</sup> 967	1.027	0.656	-0.019	-0.745	3
31274	1.184	0.720	0.133	-0.288	5
31869	1.164	0.695	0.101	-0.411	3
36552	1.144	0.662	0.130	-0.467	4
40402	1.150	0.701	0.105	-0.400	3
49960	1.202	0.737	0.144	-0.232	3
54627	1.170	0.739	0.156	-0.273	3
56438	1.197	0.741	0.124	-0.267	3
67728	1.262	0.841	0.258	-0.222	2
78146	1.235	0.846	0.218	-0.108	2
82595	1.184	0.774	0.148	-0.172	2
91805	1.168	0.692	0.132	-0.331	3
94956	1.182	0.715	0.122	-0.325	3
102851	1.208	0.766	0.124	-0.236	2
CD-37 <sup>o</sup> 7613	1.182	0.743	0.123	-0.308	2
105783	1.240	0.764	0.119	-0.257	3
120170	1.169	0.677	0.118	-0.399	1
120213	1.375	1.048	0.229	0.139	2
<s.e.>	.006	.010	.008	.010	

The Fe I curves of growth for HD 91805 and HD 100407 are illustrated in Figures 1a and 1b, respectively. No relative horizontal shift is seen in these figures, and taking this together with the identical temperature derived for these two stars, one concludes that they have the same iron abundance. This will be shown below to be solar to within  $\pm 0.2$  dex, the accuracy of the method.

Only limited spectroscopic data were obtained for HD 28307. The equivalent widths of all available lines on our plates are plotted in Figure 2 against the

values given by Griffin (1969). The agreement is good, and attests to the reliability of our line strength measurements. We have accordingly constructed the Fe I curve of growth for HD 28307 by using Griffin's equivalent widths for the lines used previously in HD 91805 and HD 100407, and show the result in Figure 1c.

The available data were not of sufficient quality for differential vertical shift measurements to be made, so that a microturbulent velocity could not be inferred. This will be considered further when we discuss the

TABLE 2  
PHOTOMETRIC AND ATMOSPHERIC DATA

HD (1)	$V$ (2)	$(R-I)_K$ (3)	$M_{bol}$ (4)	$T_{eff}$ (5)	[Fe/H] (6)	$\log g_{group}$ (7)	$\log g_{sp}$ (8)
28307.....	3.83*	0.325*	0.60*	5000	0.1†	2.8	...
91805.....	6.10‡	0.35§	...	4850	0.0	...	2.0
100407.....	3.55*	0.35*	-0.05*	4850	0.0	2.5	2.2

\* From Eggen 1972.

† From Griffin 1969.

‡ From Dean *et al.* 1977.

§ From Eggen (private communication) and the present authors.

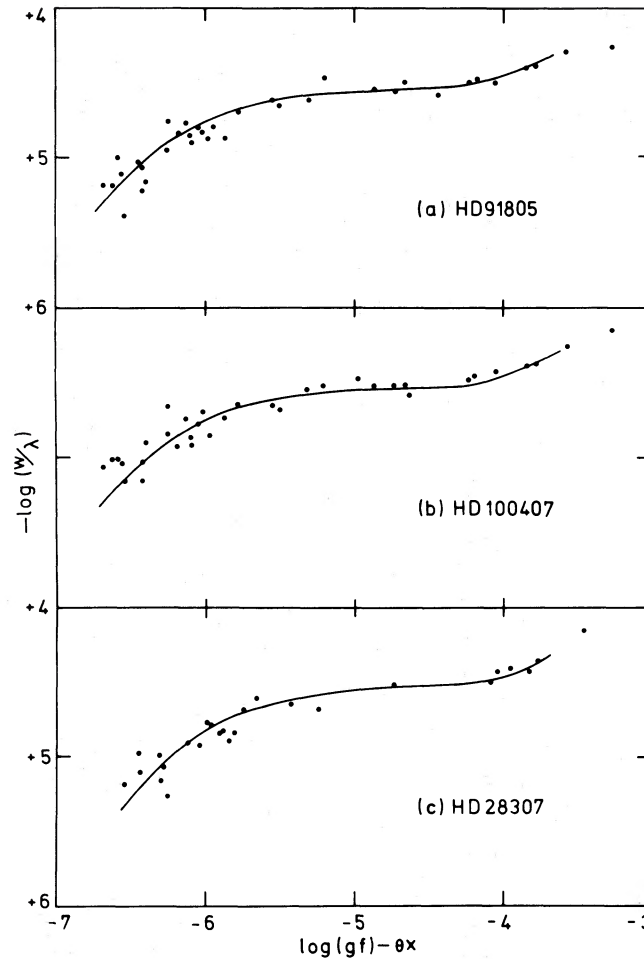


FIG. 1.—Fe I curve of growth. (a) HD 91805; (b) HD 100407; (c) HD 28307.

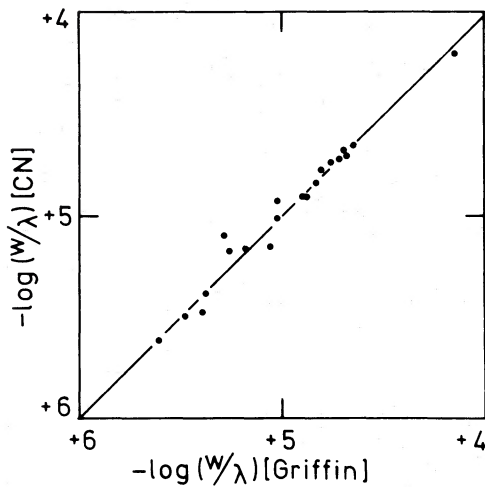


FIG. 2.—Comparison of equivalent widths for HD 28307. [CN] = Cottrell and Norris (this work); [Griffin] = Griffin (1969).

model atmospheres. We assume here that the micro-turbulence is the same in all three stars.

We now determine the iron abundances in HD 91805 and HD 100407 relative to HD 28307. On the basis of Griffin (1969), the atmosphere of HD 28307 may be represented by the following parameters:  $\theta = 1.02$ ,  $\log P_e = 2.43$ , and  $[\text{Fe}/\text{H}](\text{HD 28307} - \odot) = +0.1$ . Considering the temperature difference between HD 28307 and both HD 91805 and HD 100407, the shift required to move the curves of growth of the latter two stars onto that of HD 28307 results in a differential iron abundance,

$$[\text{Fe}/\text{H}](\{\text{HD 100407, HD 91805}\} - \text{HD 28307}) = -0.1,$$

and thus a solar iron abundance for the weak-G-band star, HD 91805. The abundances for all three stars are given in column (6) of Table 2. In what follows we assume that this result applies to all elements in the atmosphere of HD 91805 with the important exceptions of carbon, nitrogen, and oxygen.

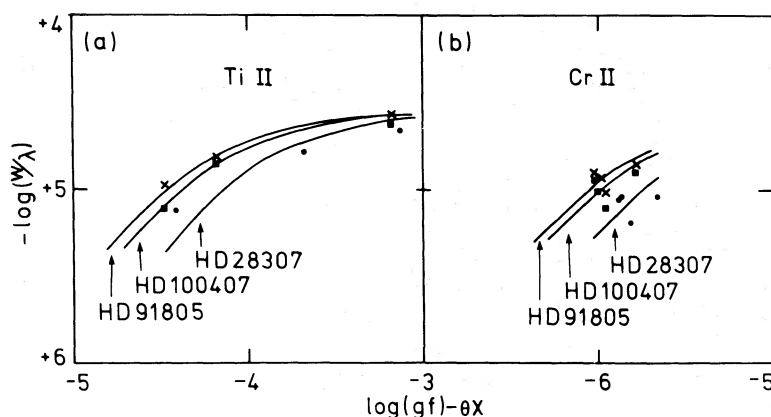


FIG. 3.—Curves of growth for ionized lines. (a) Ti II, (b) Cr II. Points for HD 28307 (●), HD 91805 (×), and HD 100407 (■) are shown. The curves are also identified.

The differential electron pressure,  $[P_e]$ , between HD 28307, HD 91805, and HD 100407 was obtained by using the ionized lines of Ti and Cr. The horizontal shift,  $[X_+]$  in the Ti II and Cr II curves of growth (Figs. 3a, 3b, respectively), was interpreted by using Pagel's (1964) relationship between this shift and  $[P_e]$ ,  $[N_j/H]$ , and  $[\theta]$ , namely,

$$[X_+] = -1.5[\theta] + \Delta\theta(-0.74) - [P_e] + [N_j/H].$$

By applying  $[g] = 2[P_e] - [x_H + Ax_m] + 1.8\Delta\theta_{\text{ion}}$ , one can obtain the differential spectroscopic gravity, where  $A$  is the overall metal abundance and  $x_H$  and  $x_m$  are the mean degrees of ionization of H and the metals. The line-forming regions of the atmospheres considered in this analysis are sufficiently cool that all the hydrogen is neutral and all the electron-contributing metals are singly ionized. This implies values of 0 and 1 for  $x_H$  and  $x_m$ , respectively.

For HD 28307 and HD 100407 using bolometric magnitudes from Eggen (1972) and assuming masses of  $\sim 2 M_\odot$  for the Hyades giants, one obtains an estimate of the gravity, shown in column (7) of Table 2. Adopting HD 28307 as the primary standard, and using the above curve-of-growth analysis, one determines spectroscopic gravities for HD 91805 and HD 100407 of 2.0 and 2.2, respectively. These are listed in column (8) of Table 2. An error,  $\pm 0.4$  dex, in the spectroscopic gravity by this method provides satisfactory agreement between this and the group membership gravity for HD 100407.

### b) Spectrum Synthesis of CH, CN, and NH

Before proceeding to our CNO abundance analysis, we will describe in detail the spectrum synthesis technique we employed.

#### i) Technique

Molecular line lists have been constructed for the ( $A^2\Delta - X^2\Pi$ ) electronic transition of CH and the blue system ( $B^2\Sigma - X^2\Sigma$ ) of CN by applying small perturbations to the formulations of Krupp (1974) and Herzberg (1955), respectively. The wavelength accuracy of all line lists, CH around  $\lambda 4300$ , CN between  $\lambda 3860$  and  $3883$  for  $\Delta v = 0$ , and also from  $\lambda 4180$  to  $4216$  for  $\Delta v = -1$ , was better than  $0.1 \text{ \AA}$ . This gave an extremely good representation of the solar spectrum.

The line strengths were calculated in parallel with the wavelength determination. The total line strength,  $f_{N'N''}$ , of a particular transition is given by

$$f_{N'N''} = \frac{\lambda_{00}}{\lambda_{N'N''}} \times f_{e1} \times q_{v'v''} \times \frac{[\text{HL}]_n}{2N'' + 1},$$

where  $N'$ ,  $N''$  are, respectively, the rotational quantum numbers of the upper and lower levels of the transition,  $\lambda_{00}$  is the band origin in  $\text{\AA}$ ,  $\lambda_{N'N''}$  is the wavelength ( $\text{\AA}$ ) of the transition,  $f_{e1}$  is the electronic oscillator strength,  $q_{v'v''}$  is the Franck-Condon factor of the vibrational band, and  $[\text{HL}]_n$  is the normalized Hönl-London factor of the individual rotational line. The sources, and in some cases the values, of the individual components of the line strength are listed in Table 3.

TABLE 3  
LINE STRENGTH DATA

Molecule	Electronic Oscillator Strength ( $f_{e1}$ )	Franck-Condon factors ( $q_{v'v''}$ )	Hönl-London factors ( $[\text{HL}]_n$ )
CH.....	$2.8 \times 10^{-3}$ Schadee 1964	Childs 1964	Schadee 1964
CN.....	$3.95 \times 10^{-2}$ Liszt and Hesser 1970	Spindler 1965	Schadee 1964

To the molecular line lists we added atomic lines from Kurucz and Peytremann (1975), according to the following selection criteria: (1) only lines of the elements calcium ( $Z = 20$ ) through to nickel ( $Z = 28$ ), and strontium ( $Z = 38$ ) to ruthenium ( $Z = 44$ ), excluding technetium ( $Z = 43$ ) were included; (2) only neutral and singly ionized lines of the above elements were retained; (3) all lines which had low excitation potentials greater than 5 eV were excluded; and (4) lines were included only if their line opacity, at a representative temperature of 5000 K in the Sun, was greater than of a line whose measured equivalent width was 15 mÅ (Moore, Minnaert, and Houtgast 1966).

Two additional line lists were constructed. The first covered the NH feature between  $\lambda\lambda 3355$  and  $3380$ , using data from Sneden (1974), while the second extended from  $\lambda\lambda 6295$  to  $6305$  to encompass the [O I] line at  $\lambda 6300.3$ .

These line lists were used in conjunction with the model-atmosphere program ATLAS (Kurucz 1970) to produce synthetic stellar spectra. One notable change was the incorporation, in data block form, of the molecular partition functions for CH, CN, and NH from Tatum (1966). These are more explicit than those calculated in ATLAS.

The molecules,  $H_2$ ,  $C_2$ ,  $N_2$ ,  $H_2O$ , CH, NH, OH, CO, and NO, were included in the equilibrium equations. These molecular species, with the exception of  $H_2$ , are competing for the available C, N, and O; all number densities are intrinsically connected.

The continuous opacity sources included were absorption by H I,  $H^-$ , He I,  $C^-$ ,  $H_2^+$ ,  $H_2^-$ , Mg I, Al I, and Si I, as well as Rayleigh scattering by H, He, and  $H_2$ , and electron scattering. Since the continuous opacity changes only slowly with wavelength, and we only compute fluxes over small wavelength intervals ( $< 50$  Å), considerable saving in computer time was made by determining this opacity only every 25 Å.

The emergent flux was calculated from the total opacity, line plus continuum, at equally spaced wavelength points over the interval requested. These fluxes were convolved with a Gaussian profile, whose width was determined by the instrument used to obtain the observational data, and with which the synthetic spectrum was compared.

Normalization of all the spectral regions, except for the NH feature around  $3360$  Å, was accomplished by taking the convolved fluxes and searching for the maximum value. All the other fluxes were then scaled accordingly. The continuum, or a point identified as a continuum point in the Arcturus atlas (Griffin 1968), was reached in all bands when the raw fluxes were convolved with a Gaussian profile of full half-width (full width at half-maximum, FWHM)  $\leq 0.6$  Å. In the region of the NH feature, heavy line blanketing makes continuum placement impossible, and comparison between theory and observation extremely difficult. We shall return to this problem in the next section.

All the model atmospheres used in this analysis are those of Bell *et al.* (1976). However, since we are considering specific temperatures, gravities, and metal abundances, subsidiary programs were written to

interpolate within this grid. At this stage we adopted a microturbulent velocity of  $2 \text{ km s}^{-1}$ , in line with the majority of the models constructed by Bell *et al.* The output from this process was in a form suitable for input into ATLAS for construction of the synthetic spectra.

Some of the semiempirical *gf*-values of Kurucz and Peytremann (1975) varied from values tabulated by other authors (Blackwell, Ibbertson, and Petford 1975; Bridges and Kornblith 1974; May, Ritcher, and Wichelmann 1974). Thus the *gf*-values were revised until the synthetic solar spectrum fitted the Utrecht Solar Atlas (Minnaert, Mulders, and Houtgast 1940). As well as these adjustments to the atomic *gf*-values, the molecular bands had to be normalized, such that the solar spectrum was reproduced. These normalization factors reflect the errors in the determination of the individual line strengths and the molecular partition functions.

#### ii) C, N, and O Abundance Analysis

The above spectrum synthesis technique has been used to determine C, N, and O abundances in the weak-G-band star HD 91805, as well as the two Hyades giant stars, HD 28307 and HD 100407.

In late-type stars where CNO abundances are solar, or near solar, carbon and oxygen are intrinsically connected in equilibrium with CO. This pertains to the Hyades giants, but in the weak-G-band star we have a simplified situation. In the latter, because of the deficiency of carbon, which we initially estimate to be a factor of 10, C and O become decoupled. For example, changing the C abundance by a factor of 2, from 1/10 to 1/20 normal, affects the [O I] line at  $\lambda 6300.3$  by less than 1%.

We begin this analysis with our oxygen abundance determination, the results of which are tabulated in column (4) of Table 4. The [O I] line equivalent widths are given in the Appendix. All abundances in Table 4 are logarithmic and relative to the Sun, for which we adopted the values of Lambert (1968). For the Hyades cluster member HD 28307, we have assumed  $[O/H] = [Fe/H]$ , as the [O I] line in our spectrum was blended with a Sc II line at  $\lambda \sim 6300.7$  Å. In the

TABLE 4  
CNO ABUNDANCES

HD (1)	[C/H]* (2)	[N/H]† (3)	[O/H] (4)
28307.....	+0.1 ± 0.2	-0.1 ± 0.3	+0.1‡
91805.....	-1.4 ± 0.3	+0.6 ± 0.4	+0.1 ± 0.2
100407.....	-0.2 ± 0.3	-0.3 ± 0.4	-0.2 ± 0.2

\* Errors in [C/H] determinations include uncertainty in the oxygen abundance, plus intrinsic errors associated with the fitting of the synthetic G-bands to the observational data.

† Errors in [N/H] include intrinsic errors due to the fitting of the synthetic spectra to the observations, as well as accumulated errors from the oxygen and carbon abundance determinations.

‡ We assume  $[O/H] = [Fe/H]$  (see text).

tracings of HD 91805 and HD 100407, this line was about the same strength as the measured [O I] line.

From the curve-of-growth analysis, the gravity produces the largest source of error,  $\pm 0.4$  dex. We therefore investigated its effect on each of our C, N, and O abundance determinations. In the weak-G-band star model atmosphere,  $\Delta \log g = 0.4$  has a 20% effect on the computed [O I] line strength, which transforms to an error in the O abundance of  $\pm 0.15$  dex.

Thus, within the limits of the method, normal oxygen abundances were obtained for HD 100407 and, in particular, HD 91805, the weak-G-band star.

Next the C abundances were computed by using CH lines within the G-band. For HD 91805 we estimate an abundance  $-1.4$  dex relative to the Sun. That is, carbon in this weak-G-band star is under-

abundant by a factor of  $\sim 25$ . Figures 4a, 4b, and 4c show both the observed and synthetic G-bands for the C abundances chosen for HD 91805, HD 28307, and HD 100407, respectively. These abundances are shown quantitatively in column (2) of Table 4.

Assigning a C abundance to the weak-G-band star is made difficult by the weakness of the CH features. In Figure 4a we include a synthetic spectrum from which the contribution of the CH molecule has been removed. The arrows in this figure indicate the spectral regions which are most sensitive to changes in the abundance. Using these regions, we estimate that  $[C/H] \sim -1.4$  gives the best fit to the observations. Deriving the C abundance in HD 91805 involved an intrinsic fitting error which was larger than those involved in determining either the O or the N

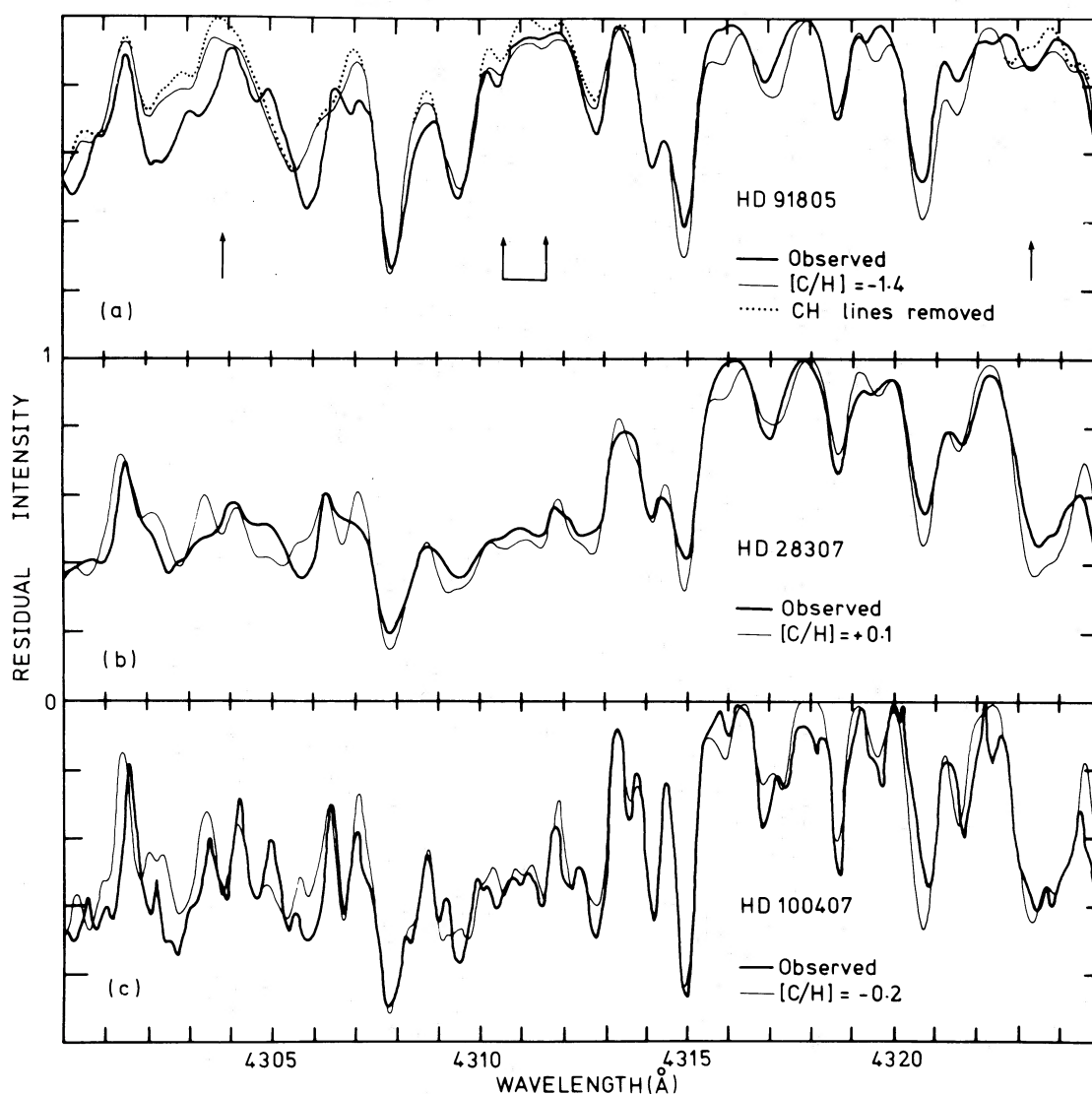


FIG. 4.—Observed and synthetic spectra for the G-band. (a) HD 91805, additional line (dots) is synthetic spectrum with no CH lines; (b) HD 28307; (c) HD 100407. The fluxes in (a) and (b) were convolved with a Gaussian profile with FWHM =  $0.6 \text{ \AA}$ . For (c), a profile with FWHM =  $0.4 \text{ \AA}$  was used (see § II).

abundances. This error propagates into the uncertainty with which we can estimate the N abundance. However, it is important to note that our procedure produces good agreement between theory and observation for both HD 28307 and HD 100407 for abundances very close to solar. Gravity variations,  $\Delta \log g = 0.4$ , have little effect,  $< 1\%$ , on the synthetic spectra, a result previously obtained by Schadee (1968).

Having evaluated carbon and oxygen abundances for the three stars, we now proceed to our determination of the nitrogen abundances, by using the CN features around  $\lambda 4200$  ( $\Delta v = -1$ ), and  $\lambda 3880$  ( $\Delta v = 0$ ). With the abundances shown in column (3) of Table 4, Figures 5a and 5b give the regions around two band heads of the  $\Delta v = -1$  system for HD 91805 and HD 28307, respectively. To emphasize the weakness of these CN bands in HD 91805, we have also shown a synthetic spectrum from which the CN contribution has been omitted. Figures 6a and 6b illustrate our results for the spectral region from  $\lambda \lambda 3870$  to  $3885$  for HD 91805 and HD 100407, respectively. Because of the greater intrinsic strength of the  $\Delta v = 0$  bands, this region provides a better discriminant for deter-

mining the nitrogen abundance. From our analysis of these two regions, we find that nitrogen is enhanced in HD 91805 by a factor  $\sim 4$  relative to the Sun, whereas abundances obtained for the two comparison stars show no deviation from normality to within the errors estimated.

It should be noted that a change in gravity of 0.4 dex alters the above features by only about 2%. Over such a small range in gravity the luminosity effect exhibited by the CN molecule is not apparent. Hence, since neither CH nor CN features are significantly affected by small changes in the gravity, once this parameter and an O abundance have been adopted, no additional errors are introduced from this source in determining the C and N abundances.

Finally, we discuss the NH feature in the near-ultraviolet. N abundances were not determined directly from this region; not only was continuum placement hopeless but also the blending of the features made identification of individual NH features impossible. Thus this spectral region was used only as a check on the results obtained by using the above CN features.

HD 91805 and HD 100407 have the same effective temperature and metal abundance, excluding C, N,

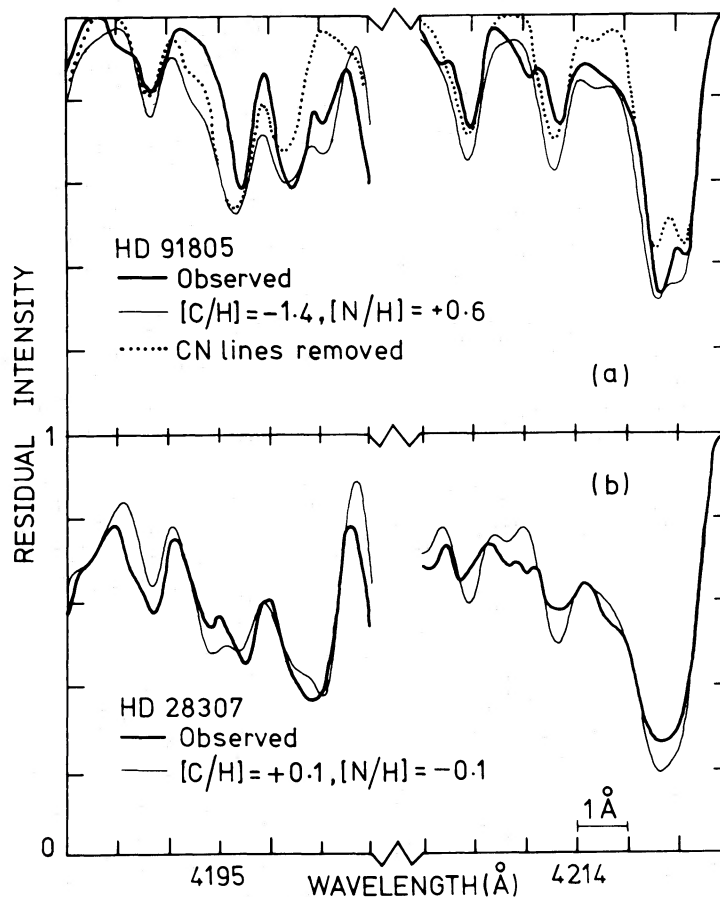


FIG. 5.—Blue CN band for  $\Delta v = -1$  system. Observations and synthetic spectra: (a) HD 91805, dotted line, synthetic spectrum with all the CN lines removed; (b) HD 28307. Convolution profile had FWHM = 0.6 Å.

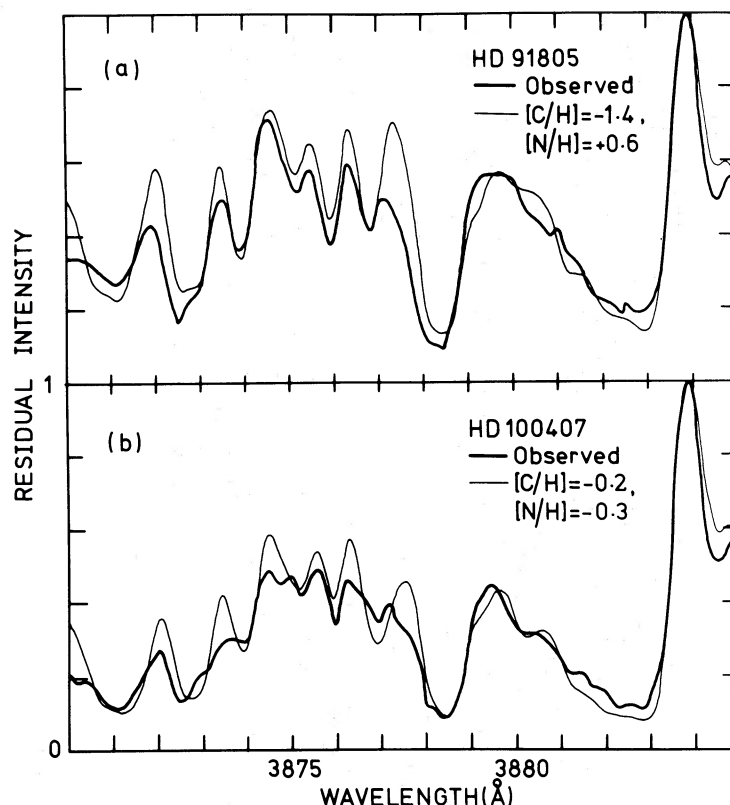


FIG. 6.—Blue CN band for  $\Delta v = 0$  for (a) HD 91805, (b) HD 100407. Convolution profile had FWHM = 0.6 Å.

and O, and only  $\Delta \log g = 0.2$ , which has little effect on the NH feature. Thus the observations of these two stars in this region can be compared directly, as shown in Figure 7. The enhanced N abundance in the weak-G-band star is apparent, but a quantitative estimate is difficult. The observed and synthetic spectra of these two stars with the nitrogen abundance adopted from the CN features are shown in Figures 8 and 8b, respectively. All the spectra shown in Figures 7 and 8 are normalized to the same point,  $\lambda \sim 3356$  Å. Although the continuum was not reached at this wavelength, normalization at this point meant that we analyzed all the data in a similar manner.

The discrepancy in Figure 8 could result from a number of effects. For the dispersions ( $10 \text{ Å mm}^{-1}$ ) and resolutions ( $\sim 1 \text{ Å}$ ) which we obtained, individual NH lines were not isolated. The measurable features are at  $\lambda \sim 3360 \text{ Å}$  and  $\lambda \sim 3370 \text{ Å}$ , with NH contributing only a portion of this absorption. Higher-dispersion observations of this region would alleviate the situation, but background fogging on the photographic plate by ion noise in the image tube would prohibit the use of the coude échelle. Therefore, the present data are the best currently obtainable at Mount Stromlo.

The other area where differences could arise is in the model atmospheric structure, particularly in the very outer surface layers, where the feature at  $\lambda \sim 3360$  is forming. This would affect the weak-G-band star

more than the Hyades giant, because of the higher N abundance and hence stronger NH lines in the former.

We also briefly investigated the lack of surface cooling by CO in HD 91805, which would result from its carbon deficiency (see Gustafsson *et al.* 1975). We increased the surface temperatures according to Figure 8 of Gustafsson *et al.*, making no attempt to adjust the other parameters, i.e.,  $P_e$ ,  $P_g$ , etc. We found

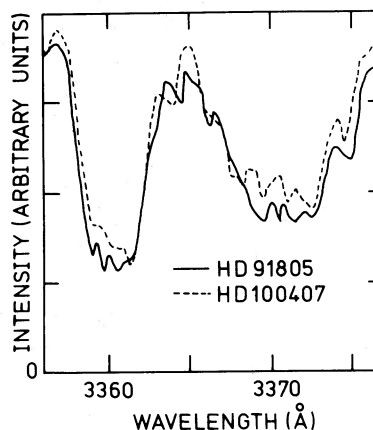


FIG. 7.—Observations for HD 91805 and HD 100407 at the near-ultraviolet NH feature.

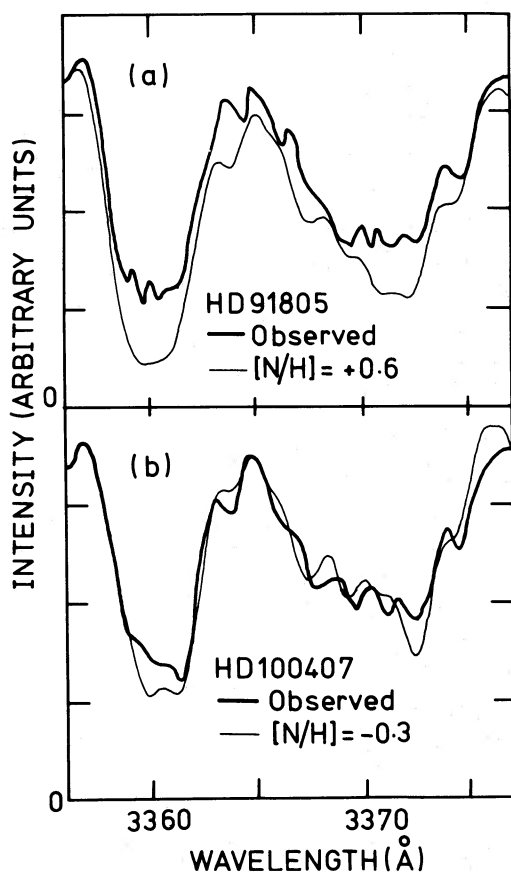


FIG. 8.—NH feature showing observed and synthetic spectra, (a) HD 91805, and (b) HD 100407. Convolution profile had FWHM = 1.5 Å.

only a slight difference in the NH feature,  $\sim 1\%$ . In view of the ad hoc nature of our method, however, it would be premature to place emphasis on this result. More work on the atmospheric structure of stars with

peculiar CNO abundances is necessary before this problem can be clarified.

The CNO abundances for HD 91805 in Table 4 are most readily explained in terms of the mixing to the surface of material processed in the CN cycle. The normal oxygen abundance implies that the NO cycle has not operated. In view of the fact that a similar result has been obtained for HR 6766 by Sneden and Peterson (1977), it seems reasonable to assume that this is a general property of the Bidelman-MacConnell weak-G-band stars. We shall now consider the possible evolutionary phases at which this peculiarity might be produced.

#### IV. THE EVOLUTIONARY STATUS OF THE BIDELMAN-MACCONNELL WEAK-G-BAND STARS

Figure 9 shows the DDO observations from Table 1 in the  $[C(45-48), C(42-45)]$ -plane, where only stars with multiple observations have been plotted, together with the Population I sequences of Osborn (1971). The most striking feature is the concentration of points at  $[C(45-48), C(42-45)] \sim (1.18, 0.72)$ .<sup>1</sup> We have also plotted in the figure the Hyades group members (Eggen 1972) for which Boyle and McClure (1975) find Hyades-like CN band strengths ( $\delta\text{CN} \geq 0.05$ ). These are stars which one may consider to be Hyades group members on both kinematic and abundance grounds. Here too we see a strong grouping (the well-known clump), at  $[C(45-48), C(42-45)] \sim (1.17, 0.82)$ . We suggest that the two groups seen in Figure 9 represent the same evolutionary phase, with the difference in position being caused by differences in CH blocking. We reason as follows. There are many CH lines in the 42 bandpass, but virtually none in

<sup>1</sup>Two stars in Table 1 deserve further investigation. BD +5°593 could be metal-weak, according to its position in both Fig. 9 and in the  $[C(38-42), C(45-48)]$ -plane. If true, it would be the brightest Population II weak-G-band star. BD -19°967 appears to be a dwarf in all DDO planes, and has the colors of a G4 V star (see Osborn 1971). It is difficult to understand G-band weakness in such an object.

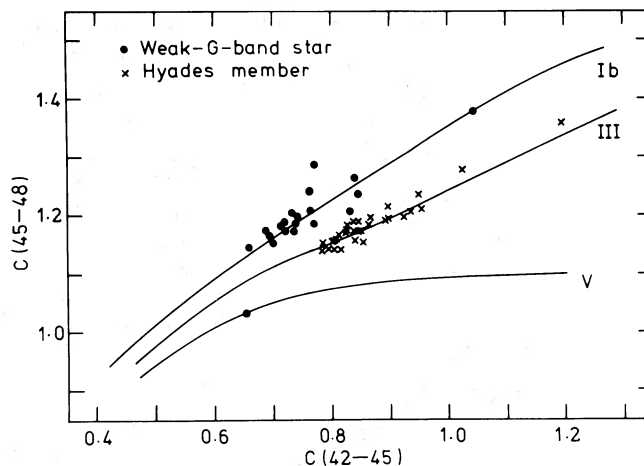


FIG. 9.—The weak-G-band stars and the Hyades group members in the  $[C(45-48), C(42-45)]$ -plane. The Population I sequences of Osborn (1971) are also shown.

either the 45 or 48 bandpasses. The color  $C(45 - 48)$  will thus be unaffected by CH blocking differences, while in the weak-G-band stars (which have less blocking in the 42 bandpass)  $C(42 - 45)$  will be somewhat bluer. We may estimate the size of the effect by comparing our spectra of the weak-G-band star HD 91805 and the Hyades cluster member HD 28307, each of which is typical of the two groupings seen in Figure 9. In particular we have blue spectra of the two stars (see § IIa) taken consecutively with the same equipment. We have used tracings of these spectra, together with the response functions of our 42 and 45 filters, to estimate the change induced in  $C(42 - 45)$  by the CH blocking around  $\lambda 4250$ . We find that HD 91805 is 0.18 and 0.04 mag bluer in the 42 and 45 bands, respectively, leading to a  $C(42 - 45)$  color bluer by 0.14 mag. The observed difference between the two stars is 0.12 mag (Table 1; Boyle and McClure 1975).

The most likely evolutionary phase of the stars in the two clumps in Figure 9 is the core helium-burning phase which follows the helium flash<sup>2</sup> (see Cannon 1970; Faulkner and Cannon 1973). We are unable to say whether the cooler and more luminous weak-G-band stars in Figure 9 are the progenitors or progeny of the clump, and will not discuss these stars further. Given, however, that most of the weak-G-band stars are burning helium in their core, it goes without saying that helium shell flashes can have little to do with G-band weakness. The same conclusion has previously been reached for Population II stars by Norris and Zinn (1977). We may also place important constraints on the masses and structure of the weak-G-band stars. For them to have experienced a core helium flash, their total mass must have been less than  $2.2 M_{\odot}$  (Iben 1967), while their helium core mass must be  $\sim 0.4$  to  $0.5 M_{\odot}$  (see Sweigart and Gross 1977). A lower limit to the total mass may be inferred from the horizontal-branch models of Gross (1973). For a metal abundance  $Z \sim 0.02$ , his results suggest that in order for such stars to fall in a clump near the giant branch, rather than at higher temperatures on a horizontal branch, the ratio of core mass to total mass must be smaller than  $\sim 0.85$ . Adopting the above core mass limits we find that this leads to a lower limit to total mass of  $\sim 0.5$ – $0.6 M_{\odot}$ . We thus have an allowed mass range  $0.5 \lesssim M/M_{\odot} \lesssim 2.2$ . The most important point that may be culled from this discussion, however, is that the weak-G-band stars have considerable envelope masses, lying in the range  $0.1$ – $1.8 M_{\odot}$ . Assuming that the weak-G-band phenomenon is not confined to the atmosphere but extends throughout the envelope, any production mechanism must have been able to process virtually all of the envelope carbon into nitrogen. This result must be achieved without processing oxygen, which—according to both Sneden and Peterson (1977)

and the present work—is normal in these stars. That is, only the CN cycle may be invoked.

There seems little reason to suspect that G-band weakness is induced during the clump phase. In § V we confine our attention to three other possible sites—the helium core flash, the red-giant branch, and the main sequence.

## V. THE ORIGIN OF THE WEAK-G-BAND PHENOMENON

### a) The Helium Core Flash

It seems difficult to reconcile the observed CNO abundances and the inferred lower limit to the envelope masses with any once-only, short-duration phenomenon such as the helium core flash. Unless the envelope is largely processed through the CN cycle at the time of the flash, which seems to us unlikely, the original carbon will still be seen in the outer layers. If the envelopes contain at least 15% of the total mass, and if before mixing the carbon abundance was normal (i.e.,  $\sim$  solar), then the final carbon abundance cannot be less than  $\sim 15\%$  solar. This is considerably larger than the observed carbon abundance.

It is perhaps important to note that this result somewhat contrasts with the opinion expressed by Norris and Zinn (1977) in their discussion of the weak-G-band effect in Population II stars. Since, however, we have no estimates of abundances in the Population II objects, we cannot yet rule out the helium core flash as the relevant phase in globular cluster evolution.

### b) The Giant Branch

There is a growing opinion that existing stellar evolution computations underestimate the amount of nuclearly processed material which is convectively mixed to the surface during the red-giant phase. Observed  $^{12}\text{C}/^{13}\text{C}$  ratios are consistently lower than predicted (Dearborn, Eggleton, and Schramm 1976, and references therein). The observed range in G-band strength on the lower giant branch of several globular clusters (Norris and Zinn 1977) is also suggestive of such a shortcoming. According to Dearborn, Eggleton, and Schramm (1976) and Norris and Zinn (1977), the most likely explanation of these phenomena lies in some combination of mass loss and possible hydrogen shell instability. We consider each in turn.

#### i) Mass Loss

Dearborn, Kozłowski, and Schramm (1976) have made the case that extensive mass loss is required in the immediate post-main-sequence phase to explain a range of astronomical observations. According to Iben (1967), a  $2.25 M_{\odot}$  star possesses a large nitrogen-rich, carbon-depleted region exterior to the hydrogen-burning regions as it leaves the main sequence. Since at this mass most energy generation on the main sequence occurs in the CN cycle, the oxygen abundance in this region is normal. Extensive mass loss at this stage could thus lead to the abundances seen in the weak-G-band stars. The Bidelman-MacConnell sample would be the stars in which the mass loss is most extreme. To explain the observations, mass must be lost right down to the enriched regions. The mass

<sup>2</sup> It should be noted that we have applied no reddening corrections to our observations. If the majority of our stars are clump objects having  $M_v \sim 0.7$  (see Eggen 1972), it obtains that they have reddenings  $E(B - V) \lesssim 0.1$  (see FitzGerald 1968, especially Fig. 1), which will have little effect on our conclusions.

fraction involved is  $\sim 0.5$ , and although such a possibility is not dismissed by Dearborn, Kozłowski, and Schramm (1976) in the context of the  $^{12}\text{C}/^{13}\text{C}$  problem, it seems to us a rather radical solution.

ii) *Instability of the Hydrogen-burning Shell*

Repeated thermal instability in the hydrogen-burning shell, and subsequent convective mixing of CN processed material to the surface, could also enhance the N/C ratio above that found in the standard computations (see Bolton and Eggleton 1973; Dearborn, Bolton, and Eggleton 1975). If, however, thermal instability exists as a universal phenomenon in all stars, one would not expect to find a large range in G-band strengths. A coupling of variable mass loss and thermal instability, on the other hand, might overcome this problem.

The present observations place important constraints on this mechanism. At the center of the hydrogen-burning shell, conditions are favorable for the ON cycle to be in equilibrium; only in the outer layers of the shell could one expect a normal oxygen abundance (Sweigart and Gross 1977). If we insist on maintaining a normal surface oxygen abundance, any mixing must therefore occur only from the outer layers of the shell. Let us suppose that the upper 1/5 of the shell is mixed to the surface during each instability, and that the envelope mass that must be processed by repeating the instability is  $0.1 M_{\odot}$ —the lower limit inferred in § IV. From Iben (1967) we estimate that a typical red giant of intermediate luminosity would have a shell of mass  $\sim 0.003 M_{\odot}$ . Then, assuming that all carbon has been transformed to nitrogen in the material to be mixed up, we estimate that some 500 instabilities are required to reduce the surface abundance to 1/20 its original value.

Dearborn, Bolton, and Eggleton (1975), on the other hand, expect  $\sim 100$  shell instabilities during the giant-branch evolution of a  $0.75 M_{\odot}$  Population II star. They note further that fewer instabilities are expected in more massive stars because of their more rapid evolution on the giant branch. We conclude that the present estimates, while rough, offer little support for thermal instability as the cause of G-band weakness.

c) *The Main Sequence and Meridional Mixing*

Paczynski (1973) has predicted that meridional circulation in rapidly rotating 3–10  $M_{\odot}$  stars can bring

CN processed material from just outside the convective core to the surface layers. In his  $3 M_{\odot}$  model, in particular, the N/C ratio increases to 200 during the main-sequence lifetime. For masses less than or equal to  $1.5 M_{\odot}$ , the mechanism fails to work because of molecular weight gradients set up by the  $p$ - $p$  cycle. No models were computed in the intermediate mass range,  $1.5 \leq M/M_{\odot} \leq 3.0$ .

The weak-G-band stars, on the other hand, have N/C  $\sim 25$ , masses less than  $\sim 2.25 M_{\odot}$ , and the low rotational velocities generally associated with late-type giants. (For HD 91805 our spectra show no line broadening relative to the Hyades giants HD 28307 and HD 100407.) Little imagination is required to see how such stars could be produced by the Paczyński mechanism. First, the abundance anomaly is produced during the main-sequence phase of rapidly rotating stars having masses greater than some critical value, lying in the range  $1.5$ – $3 M_{\odot}$ . The Bidelman-MacConnell weak-G-band stars probably represent the extreme N/C enhancement and most likely correspond to the most rapidly rotating main-sequence stars. The oxygen abundance, of course, would be normal. Second, the red-giant phase is accompanied by considerable loss of mass and angular momentum, reducing the mass (if necessary) below that required for the helium core flash, and the angular momentum to the low value observed at present. The association of rotation and loss of mass and angular momentum in the red-giant phase is not new, and has been previously invoked to explain the low rotational velocities universally observed in late-type giants, some of which must have been rapidly rotating while on the main sequence (Kraft 1970; Strittmatter and Norris 1971).

Of the several mechanisms we have considered, meridional mixing alone invokes no radical postulates and violates none of the observational constraints. It should be noted, however, that such a process cannot be invoked to explain the G-band weakness observed in globular cluster giants, which have masses considerably smaller than those considered here.

P. L. Cottrell wishes to acknowledge the support of an Australian National University Postgraduate Award, which enabled us to have access to the UNIVAC 1100/42 computer, operated by the Australian National University Computer Center.



- Iben, I., Jr. 1967, *Ap. J.*, **147**, 650.  
 Johnson, H. L. 1966, *Ann. Rev. Astr. Ap.*, **4**, 193.  
 Kraft, R. P. 1970, in *Spectroscopic Astrophysics: An Assessment of the Contributions of Otto Struve*, ed. G. H. Herbig (Berkeley: University of California Press), p. 385.  
 Krupp, B. M. 1974, *Ap. J.*, **189**, 389.  
 Kurucz, R. L. 1970, "Smithsonian Ap. Obs. Spec. Rept.," No. 309.  
 Kurucz, R. L., and Peytremann, E. 1975, "Smithsonian Ap. Obs. Spec. Rept.," No. 362.  
 Lambert, D. L. 1968, *M.N.R.A.S.*, **138**, 143.  
 Liszt, H. S., and Hesser, J. E. 1970, *Ap. J.*, **159**, 1101.  
 Mallia, E. A. 1975, *M.N.R.A.S.*, **170**, 57P.  
 May, M., Ritcher, J., and Wichelmann, J. 1974, *Astr. Ap. Suppl.*, **18**, 405.  
 McClure, R. D. 1976, *A.J.*, **81**, 182.  
 Minnaert, M., Mulders, G. F. W., and Houtgast, J. 1940, *Photometric Atlas of the Solar Spectrum* (Amsterdam: Schnabel).  
 Moore, C. E., Minnaert, M. G. J., and Houtgast, J. 1966, NBS Monograph, No. 61.  
 Norris, J., and Bessell, M. S. 1977, *Ap. J. (Letters)*, **211**, L91.  
 Norris, J., and Zinn, R. 1977, *Ap. J.*, **215**, 74.  
 Osborn, W. 1971, Ph.D. thesis, Yale University.  
 Paczyński, B. 1973, *Acta Astr.*, **23**, 191.  
 Pagel, B. E. J. 1964, *Roy. Obs. Bull.*, No. 87.  
 Schadee, A. 1964, *Bull. Astr. Inst. Netherlands*, **17**, 311.  
 ———. 1968, *Ap. J.*, **151**, 239.  
 Sneden, C. 1974, Ph.D. thesis, University of Texas at Austin.  
 Sneden, C., and Peterson, R. 1977, *Bull. AAS*, **9**, 365.  
 Spindler, J. R. 1965, *J. Quant. Spectrosc. Rad. Transf.*, **5**, 165.  
 Strittmatter, P. A., and Norris, J. 1971, *Astr. Ap.*, **11**, 477.  
 Sweigart, A. V., and Gross, P. G. 1977, preprint.  
 Tatum, J. B. 1966, *Pub. Dom. Ap. Obs.*, Vol. **13**, No. 1.  
 Weast, R. C. 1965, *Handbook of Chemistry and Physics* (Cleveland: Chemical Rubber Co.), p. E-143.  
 Zinn, R. 1973, *Ap. J.*, **182**, 183.  
 ———. 1977, *Ap. J.*, **218**, 96.

P. L. COTTRELL and JOHN NORRIS: Mount Stromlo and Siding Spring Observatory, Private Bag, Woden P.O., A.C.T., Australia 2606